Complex networks with complex weights

Lucas Böttcher[1,2,*] and Mason A. Porter[3,4,5,†]

[1]*Department of Computational Science and Philosophy, Frankfurt School of Finance and Management, 60322 Frankfurt am Main, Germany*
[2]*Department of Medicine, University of Florida, Gainesville, Florida, 32610, USA*
[3]*Department of Mathematics, University of California, Los Angeles, California 90095, USA*
[4]*Department of Sociology, University of California, Los Angeles, California 90095, USA*
[5]*Santa Fe Institute, Santa Fe, New Mexico 87501, USA*

(Received 15 December 2022; revised 25 July 2023; accepted 20 December 2023; published 27 February 2024)

In many studies, it is common to use binary (i.e., unweighted) edges to examine networks of entities that are either adjacent or not adjacent. Researchers have generalized such binary networks to incorporate edge weights, which allow one to encode node–node interactions with heterogeneous intensities or frequencies (e.g., in transportation networks, supply chains, and social networks). Most such studies have considered real-valued weights, despite the fact that networks with complex weights arise in fields as diverse as quantum information, quantum chemistry, electrodynamics, rheology, and machine learning. Many of the standard network-science approaches in the study of classical systems rely on the real-valued nature of edge weights, so it is necessary to generalize them if one seeks to use them to analyze networks with complex edge weights. In this paper, we examine how standard network-analysis methods fail to capture structural features of networks with complex edge weights. We then generalize several network measures to the complex domain and show that random-walk centralities provide a useful approach to examine node importances in networks with complex weights.

DOI: 10.1103/PhysRevE.109.024314

I. INTRODUCTION

Network analysis has provided useful insights into many physical, biological, and social phenomena [1]. There has been a wealth of research both about network structure and about the effects of network structure on dynamical processes (including opinions and social influence, the spread of infectious diseases, and synchronization) [2]. If information about the intensity of interactions (and hence about the coupling strengths) between nodes is unavailable, unweighted networks provide a reasonable starting point to study structural features of systems in which one can describe nodes as either in contact (or otherwise interacting) or not in contact. However, in many applications, it is useful to use edge weights to account for the intensities or frequencies of interactions between nodes. For example, researchers have used weighted edges to describe the contact frequencies between individuals in human social networks [3], passenger flows in air-transportation networks [4], interactions between different parts of a protein molecule [5], and much more.

The vast majority of research on weighted networks has focused on networks with real-valued edge weights [4,6–9] and node weights [10]. However, networks with complex weights arise in many scientific and engineering applications (see Table I), and it is necessary to adapt and reformulate existing network-analysis methods to study them. In the present paper, we extend ideas from the analysis of network structure to networks with complex weights.

In quantum physics [11–13], one defines wave functions and their unitary evolution in complex vector spaces. Recent experiments provide strong evidence that real-valued formulations of the standard framework of quantum physics [14] fail to capture physical reality [15–17]. In classical physics (e.g., in fluid dynamics and electrodynamics), complex values allow one to simplify mathematical descriptions of wave-like phenomena. Additionally, researchers in machine learning, neuroinformatics, and allied subjects have a long history of exploiting complex-valued weights in the analysis and application of artificial neural networks [18–20]. Researchers have also examined the effects of complex weights in models of biological neuronal dynamics [21,22].

Network analysis has yielded insights into individual quantum systems, quantum networks that one can construct using entangled states or physically interconnected systems, and a variety of other quantum phenomena [70,71]. In quantum physics, one can think of Hermitian matrices that are associated with the Hamiltonian of an isolated quantum system as an adjacency matrix with real-valued diagonal terms (i.e., energy terms) and complex-valued off-diagonal terms, which describe changes in amplitude during a transition from one state to another state. The connection between modularity maximization and node-occupation properties of random walks has been used to identify communities in such networks [72]. Complex weights also arise in interferometer networks [73], Dirac equations on networks [74,75], quantum cellular automata [76], and "Vdovichenko's method" [77] to derive random-walk–based solutions of the Ising model on a two-dimensional (2D) lattice [78,79].

In electrodynamics, one can interpret a network with real-valued edge weights as a network of resistors with weights

*l.boettcher@fs.de
†mason@math.ucla.edu

TABLE I. Summary of a variety of application areas of networks with complex weights. For the indicated applications in electrostatics and rheology (which we mark with *), one can use complex node weights to describe heterogeneous materials that are subject to heterogeneous electromagnetic and force fields. All other listed applications primarily use edge weights. A ✓ indicates that a subject includes examples with Hermitian weight matrices, and a ✗ indicates that a subject includes examples with non-Hermitian weight matrices.

Subject	Some applications	$W = W^\dagger$	References
Quantum information	Description of quantum walks	✓	[23–31]
Condensed-matter physics	Electron transport in quantum networks; Interactions between electrons and magnetic fields	✗✓	[32–35]
Mathematical chemistry	Structural properties of molecules	✗✓	[36–38]
Electrodynamics	Impedance values, reflection coefficients, and transmission coefficients in transmission-line networks	✗	[39–47]
Electrostatics	Complex permittivities and permeabilities*	✗	[39]
Rheology	Complex storage and loss moduli of viscoelastic materials*	✗	[48]
Computational social science	Social-network analysis	✓	[49,50]
Machine learning	Complex-valued neural networks; Graph neural networks; Graph signal processing; Sparsification of magnetic Laplacians	✗✓	[51–65]
Linear algebra	Hermitian directed graphs	✓	[66–69]

that encode resistance values. One can use complex weights to describe impedance and admittance values in more general transmission-line networks, such as in lumped-element models of coupled transmission lines that include resistors, coils, and capacitors [40–47].

In applications of machine learning, allowing edge weights to take complex values can substantially improve the performance of artificial neural networks. In comparison to their real-valued counterparts, complex-valued neural networks can have better accuracies, convergence properties, and capacities to produce nonlinear decision boundaries (even for small numbers of neurons) [58].[1] A variant of complex-valued neural networks called "phasor neural networks" have been used to construct associative memory [51–53], and a complex-valued generalization of the original Hopfield network [80–82] has been trained in image-retrieval tasks using Hebbian learning [57]. To train complex-valued artificial neural networks with gradient-based methods, researchers developed a version of the backpropagation algorithm that can update complex-valued weights and biases [54,55].

In Table I, we indicate several application areas of networks with complex edge weights and/or complex node weights. This table does not give a rigid classification; instead, it illustrates a variety of areas in which networks with complex weights arise. Because of the connection between complex adjacency matrices and network descriptions of quantum transport of charged particles [34,83], some researchers refer to a complex adjacency matrix as a "magnetic adjacency matrix" in this context [84–86]. One can use a complex adjacency matrix to construct a "magnetic Laplacian", which has been used for applications such as graph visualization [87] and has been integrated into graph neural networks to study node classification and edge inference (i.e., "edge prediction") in directed networks [60,61]. Researchers have also examined sparsification of magnetic Laplacians [65], and a recent study [50] examined the spectral properties of magnetic Laplacians that are associated with networks with complex weights. Many of the works that we list in Table I focus on Hermitian weight matrices W (i.e., weighted adjacency matrices that satisfy $W = W^\dagger$). Complex weight matrices in electrodynamics, electrostatics, and materials science may not be Hermitian, as they describe heterogeneous materials or materials that are subject to heterogeneous fields [39,48]. Non-Hermitian weight matrices also arise in multi-agent control [88,89].

In the present paper, we examine several issues with the application of standard network-analysis methods to networks with complex weights. We also explore a variety of connections to physical systems that help us interpret the meaning of complex weight matrices.

In Sec. II, we give a mathematical definition of networks with complex weights and we then discuss the relationship between such networks and random walks and opinion consensus [90]. As analogs of classical random walks and DeGroot consensus dynamics, we show that Hermitian complex weight matrices induce continuous-time quantum walks (CTQWs) and phase-synchronization dynamics that are related to the Schrödinger–Lohe model, which is a generalization of Kuramoto dynamics to non-Abelian oscillators and quantum oscillators [91–95]. In Sec. III, we identify another connection to phase synchronization by defining appropriate local network measures [4], such as a complex-valued node strength and a complex-valued weighted clustering

[1]For example, one can use a single layer with two complex-valued neurons to represent conic sections (i.e., parabolas, ellipses, and hyperbolas). A single layer with two real-valued neurons can only represent linear functions [58,59].

coefficient. Importantly, although there exist connections between various dynamical systems and networks with complex weights, the evolution of a dynamical system on a network depends not only on an underlying weight matrix but also on the specific interaction rules that characterize that system [2]. Nevertheless, as illustrated by several decades of research in network analysis, analyzing the mathematical properties (e.g., the spectra) of adjacency matrices and weight matrices can yield crucial insights into the stability and other properties of networked dynamical systems [1,96].

In Sec. IV, we extend our discussion of walks on networks with complex weights and explain that one can interpret walks and their associated complex weights in terms of (1) interactions between charged particles and a magnetic field [34] and (2) exchange statistics of indistinguishable particles [97–101]. To mathematically characterize the structural differences between networks with binary, real, and complex edge weights, we study how different weight matrices affect graph energy (i.e., the sum of the absolute values of the eigenvalues of W) in Sec. V. Graph energy is a common network measure in mathematical chemistry because of its connection to π-electron energy in tight-binding models [102].

One cannot directly apply certain network notions (such as eigenvector centrality and its generalizations) to networks with complex edge weights, as one must first have a matrix—either a weight matrix or some other matrix, such as a function of a weight matrix—that satisfies the Perron–Frobenius theorem [103,104], for which one seeks a real-valued and positive matrix to ensure a leading eigenvector with strictly positive entries. In Sec. VI, we discuss generalizations of the Perron–Frobenius theorem [105,106] and eigenvector centrality. The inability to fully order complex numbers forces one to appropriately adapt other centrality measures if one desires to employ them. This issue becomes apparent for concepts like geodesic centrality measures, which are based on shortest paths. Approaches to compute such measures with Dijkstra's algorithm (when edge weights are positive) or the Bellman–Ford algorithm (when edge weights are either positive and negative) rely on comparing ordered quantities [107,108]. In Sec. VII, we examine random-walk centrality measures that allow both real-valued and complex-valued edge weights [28,109]. We thereby work with appropriate notions of centrality that allow us to avoid this issue. Finally, in Sec. VIII, we discuss our results and indicate some future directions in the study of networks with complex weights. Our code is publicly available at [110].

II. COMPLEX WEIGHTS AND THEIR CONNECTION TO RANDOM WALKS AND OPINION CONSENSUS

We consider networks in the form of weighted graphs $G = (V, E, w)$, where V is a set of nodes, E is a set of edges, and the function $w : E \to \mathbb{C}$ assigns a complex weight to each edge. The number of nodes is $N = |V|$. We use both an adjacency matrix $A \in \{0, 1\}^{N\times N}$ and a weight matrix (i.e., a weighted adjacency matrix) $W \in \mathbb{C}^{N\times N}$ to describe weighted edges between nodes. The entries a_{ij} of the matrix A are equal to 1 if nodes i and j are adjacent and are equal to 0 if they are not adjacent. Unless we state otherwise, we do not consider self-edges or self-weights. (That is, we take $a_{ii} = w_{ii} = 0$.) To capture complex-valued relationships between nodes, we let the weight-matrix entries $w_{ij} = r_{ij}e^{i\varphi_{ij}}$ be complex numbers with magnitude r_{ij} and phase φ_{ij}. If a network is undirected, then $a_{ij} = a_{ji}$, $r_{ij} = r_{ji}$, and $\varphi_{ij} = \varphi_{ji}$. If $a_{ij} = 0$, we set $w_{ij} = 0$. In Fig. 1, we show examples of networks with real and complex weights. Both of the depicted networks are "closed" (i.e., all edges are present) and directed triads. (A "triad" is a subgraph of a network that consists of three nodes.)

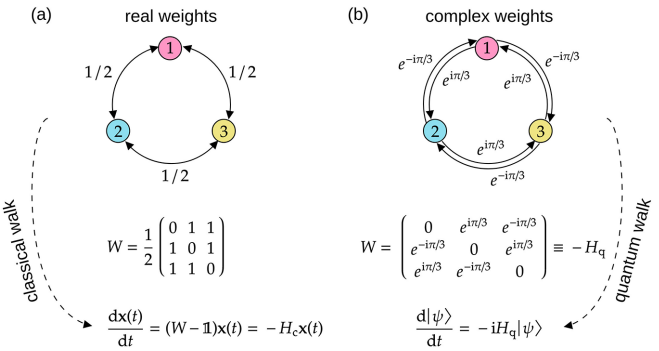

FIG. 1. Examples of networks with real and complex edge weights. Each of these networks is a closed and directed triad. (a) The weight matrix W is stochastic. It induces random-walk dynamics $\dot{\mathbf{x}}(t) = -H_c\mathbf{x}(t)$, where $H_c = \mathbb{1} - W$ and $\mathbf{x}(t)$ is a probability vector whose entries $x_i(t)$ (with $i \in \{1, 2, 3\}$) give the probabilities of finding a random walker at each node i at time t. (b) The weight matrix W is Hermitian. It induces a continuous-time quantum walk $|\dot{\psi}\rangle = -iH_q|\psi\rangle$, where $|\psi\rangle \in \mathbb{C}^3$ and $H_q = -W$.

A. Weighted networks and linear diffusion dynamics

For a strongly connected network with non-negative and symmetric real weights w_{ij} [see Fig. 1(a)], we can rescale w_{ij} by mapping $w_{ij} \to w_{ij}/(\sum_{j=1}^{N} w_{ij})$ to obtain a stochastic weight matrix that induces the random-walk dynamics

$$\frac{d\mathbf{x}(t)}{dt} = (W - \mathbb{1})\mathbf{x}(t) = -H_c\mathbf{x}(t)\,, \tag{1}$$

where $H_c = \mathbb{1} - W$ is the classical (as opposed to quantum) random-walk Hamiltonian, $\mathbb{1}$ is the identity matrix, and $\mathbf{x}(t)$ is a probability vector with entries $x_i(t)$ (with $i \in \{1, \ldots, N\}$), which give the probabilities of finding a random walker at each node i at time t. Under the aforementioned weight rescaling, one can thus always interpret a strongly connected network with non-negative and symmetric real weights in terms of transition probabilities of a classical random walker. In the present paper, we consider specific choices of H_c that are associated with left-stochastic and right-stochastic weight matrices.

For the left-stochastic weight matrix $W = AD^{-1}$ in an undirected network (i.e., a network with $a_{ij} = a_{ji}$ for all i and j), we obtain $H_c = LD^{-1}$, where $L = D - A$ is the combinatorial graph Laplacian, $D = \mathrm{diag}(k_1, \ldots, k_N)$ is the degree matrix, and $k_i = \sum_j a_{ij}$ is the degree of node i (i.e., the number of neighbors of node i). The stationary state of Eq. (1)

for $H_c = LD^{-1}$ yields an occupation-centrality measure that is proportional to node degree [28,111].

The random-walk evolution (1) is equivalent to the continuous-time DeGroot opinion-consensus model

$$\frac{dx_i(t)}{dt} = \sum_{j=1}^{N} a_{ij}[x_j(t) - x_i(t)] \tag{2}$$

if we replace $H_c = LD^{-1}$ with $H_c = L$ [112,113]. In the DeGroot model, we treat the underlying network as undirected and $x_i(t)$ is the opinion of node i.

For the right-stochastic weight matrix $W = D^{-1}A$ in an undirected network, we obtain

$$\frac{dx_i(t)}{dt} = \sum_{j=1}^{N} w_{ij}[x_j(t) - x_i(t)] \tag{3}$$

as a generalization of Eq. (2). As in the original continuous-time DeGroot model (2), the nontrivial stationary state $\mathbf{x}^*$ of the weighted-network generalization (3) is a consensus state, which entails that $x_i^* = x_j^* \equiv x^*$ for all nodes i and j. Unlike in Eq. (2), the quantity $\sum_i x_i(t)$ is, in general, not conserved in Eq. (3) because a right-stochastic weight matrix is symmetric only for regular graphs (i.e., for graphs in which each node has the same degree).

One can also establish a connection between weighted networks and linear diffusion dynamics for networks with complex weights [114]. A Hermitian weight matrix W (i.e., a weight matrix that satisfies $W = W^\dagger$) induces a CTQW that evolves according to the Schrödinger equation

$$\mathrm{i}\frac{d\,|\psi\rangle}{dt} = H_q\,|\psi\rangle\,, \tag{4}$$

where $|\psi\rangle \in \mathbb{C}^N$ and $H_q = -W$ [see Fig. 1(b)]. The Hamiltonian H_q is the generator of time translation of a CTQW.

We use bra–ket notation. In an N-dimensional Hilbert space (e.g., $\mathbb{C}^N$ equipped with the standard Hermitian inner product), a "ket" $|\psi\rangle$ is a column vector and a "bra" $\langle\psi|$ is the conjugate transpose of $|\psi\rangle$. The elements of the row vector $\langle\psi|$ are thus complex conjugates of the corresponding elements of $|\psi\rangle$. As usual, $\langle\psi|\phi\rangle$ denotes the inner product that is associated with $|\psi\rangle, |\phi\rangle \in \mathbb{C}^N$. The norm of $|\psi\rangle$ is $\|\psi\|^2 = \langle\psi|\psi\rangle$, and the outer product of the vectors $|\psi\rangle$ and $|\phi\rangle$ is $|\psi\rangle\langle\phi|$. In an N-dimensional vector space, the outer product is an $N \times N$ matrix.

The infinite-time mean

$$\pi_j = \lim_{T\to\infty} \frac{1}{T}\int_0^T \langle j|\rho(t)|j\rangle\, dt \tag{5}$$

of a CTQW gives an occupation-centrality measure for a network with complex edge weights [111]. In Eq. (5), dt is an infinitesimal time step, $\rho(t) = |\psi(t)\rangle\langle\psi(t)|$ is a density operator, and $|j\rangle \in \mathbb{C}^N$ is an orthonormal basis vector and hence satisfies

$$\langle i|j\rangle = \delta_{ij}\,. \tag{6}$$

B. Consensus dynamics, the Schrödinger–Lohe model, and synchronization

We obtain a quantum-mechanical analog of the DeGroot consensus dynamics (2) by setting

$$(H_q)_i = \mathrm{i}\sum_{j=1}^{N} a_{ij}[|\psi_j\rangle\langle\psi_i| - |\psi_i\rangle\langle\psi_j|]\,, \tag{7}$$

which yields

$$\mathrm{i}\frac{d\,|\psi_i\rangle}{dt} = \mathrm{i}\sum_{j=1}^{N} a_{ij}[|\psi_j\rangle - \langle\psi_j|\psi_i\rangle\,|\psi_i\rangle]\,. \tag{8}$$

Equation (8) preserves $\|\psi_i\|^2 = \langle\psi_i|\psi_i\rangle$ for each state $|\psi_i\rangle \in \mathbb{C}$ (see Appendix A) and synchronizes the relative phases between the states $|\psi_i\rangle$ and $|\psi_j\rangle$ (with $i \neq j$). It is the special case of the Schrödinger–Lohe model [91,92] with the Hamiltonian (7). Other versions of the Schrödinger–Lohe model include a Laplacian term in the Hamiltonian. These versions include variants with an additional potential function [94] and variants without one [93].

If a state $|\psi_i\rangle$ satisfies $\|\psi_i\|^2 = 1$, then $|\psi_i\rangle = e^{-\mathrm{i}\theta_i(t)}$. After the rescaling $a_{ij} \to a_{ij}K/(2N)$, the dynamical system (8) is equivalent to the Kuramoto model

$$\frac{d\theta_i(t)}{dt} = \frac{K}{N}\sum_{j=1}^{N} a_{ij}\sin[\theta_j(t) - \theta_i(t)]\,, \tag{9}$$

with a homogeneous coupling constant K and a rotating reference frame in which all oscillators have the same natural frequency [115]. The continuous-time DeGroot model (2) corresponds to the linearization of Eq. (9) for small phase differences and $K = N$. Lohe's generalization of Kuramoto dynamics to non-Abelian oscillators and quantum oscillators [91–95] is also related to recent work on Kuramoto dynamics on high-dimensional spheres [116] and with complex phases [117].

In a network with complex edge weights, we examine a weighted variant of the Hamiltonian (7). This variant is

$$(H_q)_i = \mathrm{i}\sum_{j=1}^{N}[w'_{ij}\,|\psi_j\rangle\langle\psi_i| - w_{ij}\,|\psi_i\rangle\langle\psi_j|]\,. \tag{10}$$

The Hamiltonian $(H_q)_i$ in Eq. (10) is Hermitian if and only if the weights w_{ij} and w'_{ij} satisfy $w_{ij} = \bar{w}'_{ij}$ (where the bar denotes complex conjugation) for all i and j. Setting $w_{ij} = Ke^{\mathrm{i}\alpha}/(2N)$ and $w'_{ij} = Ke^{-\mathrm{i}\alpha}/(2N)$ for all i and j yields the Sakaguchi–Kuramoto (SK) model[2]

$$\frac{d\theta_i(t)}{dt} = \frac{K}{N}\sum_{j=1}^{N} a_{ij}\sin[\theta_j(t) - \theta_i(t) + \alpha]\,, \tag{11}$$

[2]We use the term "Sakaguchi–Kuramoto model" because Ref. [118] lists Sakaguchi and Kuramoto as first and second authors, respectively. Some researchers use the term "Kuramoto–Sakaguchi model" to refer to this model.

where α is a phase lag and $|\alpha| \leqslant \pi/2$ [118]. Analogously to Eq. (9), we can interpret Eq. (11) as describing the evolution of coupled Sakaguchi–Kuramoto oscillators with the same natural frequencies in a rotating reference frame. Many researchers have examined identical Kuramoto oscillators and identical Sakaguchi–Kuramoto oscillators in a rotating reference frame; see, e.g., Refs. [119–122]. The empirical motivation of the phase-lag parameter α is that the common frequency of strongly coupled oscillators typically deviates from the mean of their natural frequencies [118]. The SK model is relevant to various applications, such as the synchronization of coupled electrical oscillators [123].

C. Quantifying classical and quantum consensus

For classical consensus dynamics like (2) and (3), we quantify the amount of consensus by calculating the order parameter

$$r_{\mathrm{c}}(t) = 1 - \frac{1}{2\Gamma}\|\mathbf{x} - \mathbf{x}^*\|_1 = 1 - \frac{1}{2\Gamma}\sum_{i=1}^{N}|x_i(t) - x^*|\,, \quad (12)$$

where $\Gamma = Nx^*$ and $\mathbf{x}^* = (x^*, \ldots, x^*)^\top$ is a consensus state.

For the unweighted DeGroot consensus model (2) with $\sum_{i=1}^{N} x_i(0) = 1$, we have $x^* = 1/N$ (with $i \in \{1, \ldots, N\}$) and $\lim_{t\to\infty} r_{\mathrm{c}}(t) = 1$. At time $t = 0$, the consensus $r_{\mathrm{c}}(0)$ reaches a minimum $1/N$ for

$$x_i(0) = \begin{cases} 1\,, & \text{if } i = i' \\ 0\,, & \text{if } i \neq i'. \end{cases} \quad (13)$$

At this minimum of $r_{\mathrm{c}}(0)$, the opinion of one node deviates maximally from the opinions of the other nodes. For the weighted DeGroot model (3), the stationary state is $\mathbf{x}^* = \lim_{t\to\infty} e^{(W-\mathbb{1})t}\mathbf{x}(0)$.

For $|\psi_i\rangle = e^{-\mathrm{i}\theta_i(t)}$, the corresponding order parameter for the quantum consensus dynamics (8) is

$$[r_{\mathrm{q}}(t)]^2 = 1 - \frac{1}{2N^2}\sum_{i,j}\|\psi_i - \psi_j\|^2 = \frac{1}{N^2}\sum_{i,j} e^{\mathrm{i}[\theta_j(t)-\theta_i(t)]}$$
$$= \frac{1}{N^2}\sum_{i,j}\cos[\theta_j(t) - \theta_i(t)]\,, \quad (14)$$

so $r_{\mathrm{q}}(t)$ is equivalent to the order parameter of the Kuramoto model [115].

In Fig. 2, we show the evolution of $r_{\mathrm{c}}(t)$ and $r_{\mathrm{q}}(t)$ for classical and quantum consensus dynamics on one network from a $G(N, p)$ Erdős–Rényi (ER) random-graph model with $N = 100$ nodes and probability $p = 0.2$ for an edge to exist between two nodes. For the weighted DeGroot model (3), we set $w_{ij} = a_{ij}/k_i$. Additionally, we set $w_{ij} = e^{-\mathrm{i}\pi/4}$ and $w'_{ij} = e^{\mathrm{i}\pi/4}$ for all i and j in the weighted Hamiltonian (10). In Fig. 2, we observe that the unweighted consensus dynamics reach values of $r_{\mathrm{c}}(t)$ and $r_{\mathrm{q}}(t)$ near 1 faster than their weighted counterparts. We also observe that the weighted quantum consensus dynamics achieves smaller consensus values than its unweighted counterpart.

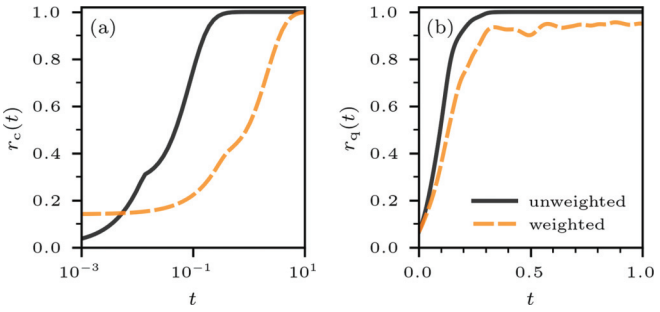

FIG. 2. Classical and quantum consensus. The evolution of the (a) classical consensus (12) and (b) quantum consensus (14). The underlying network is one network from a $G(N, p)$ Erdős–Rényi (ER) random-graph model with $N = 100$ nodes and connection probability $p = 0.2$. The solid black curves indicate the amount of consensus in the unweighted models, and the dashed orange curves indicate the amount of consensus in the weighted models. For the weighted DeGroot model (3), we set $w_{ij} = a_{ij}/k_i$. Additionally, we set $w_{ij} = e^{-\mathrm{i}\pi/4}$ and $w'_{ij} = e^{\mathrm{i}\pi/4}$ for all i and j in the weighted Hamiltonian (10). In panel (a), we compute $\mathbf{x}(t)$ in $r_{\mathrm{c}}(t)$ by evaluating $e^{(W-\mathbb{1})t}\mathbf{x}(0)$, where $x_1(0) = 1$ and $x_j(0) = 0$ for $j \in \{2, \ldots, N\}$. In panel (b), we use an implicit unitary integrator to solve Eq. (4) with the Hamiltonian (10). We normalize each initial wave-function component $|\psi_i(0)\rangle$ (with $i \in \{1, \ldots, N\}$) to 1, and we uniformly randomly distribute their phases with mean $\pi/3$ and variance $25/3$.

III. LOCAL NETWORK MEASURES

Because the entries w_{ij} of W are complex-valued, the strength (i.e., weighted degree)

$$s_i = \sum_{j=1}^{N} w_{ij} \quad (15)$$

of node i is also a complex-valued quantity. In contrast to situations with real-valued edge weights [4], s_i does not provide a measure of importance or centrality of node i because one cannot fully order complex numbers.

To quantify the distribution of the complex weights of the edges that are attached to node i, we define the normalized strength of node i as

$$\bar{s}_i = \frac{s_i}{k_i} = \frac{\sum_{j=1}^{N} w_{ij}}{\sum_{j=1}^{N} a_{ij}}\,. \quad (16)$$

How do different values of the amplitudes r_{ij} and phases φ_{ij} affect the value of $\bar{s}_i$? To answer this question, we first suppose that $r_{ij} = 1$ for all i and j. For $a_{ii} = w_{ii} = 0$ and $r_{ij} = 1$, we have

$$\bar{s}_i = \frac{1}{k_i}\sum_{j=1}^{N} a_{ij} e^{\mathrm{i}\varphi_{ij}}, \quad (17)$$

so

$$|\bar{s}_i|^2 = \frac{1}{k_i^2}\sum_{j,l} a_{ij}a_{il}e^{\mathrm{i}(\varphi_{ij}-\varphi_{il})}$$
$$= \frac{1}{k_i^2}\sum_{j,l} a_{ij}a_{il}\cos(\varphi_{ij} - \varphi_{il})\,. \quad (18)$$

Equation (18) implies that $|\bar{s}_i|^2$ resembles the order parameter of the Kuramoto model [see Eq. (14)]. Observe that $|\bar{s}_i|^2 = 1$ if $\varphi_{ij} = \varphi_{il}$ whenever $a_{ij}a_{il} > 0$ (i.e., for all edges that are attached to node i) and that $\bar{s}_i$ reaches its minimum value 0 if all phases are balanced around the unit circle (i.e., if they are spread evenly or distributed in clusters that balance each other).

If $r_{ij} = r$, then $0 \leqslant |\bar{s}_i|^2 \leqslant r^2$. Additionally, for general distributions of r_{ij} with $r_{\max} = \max_{i,j}(r_{ij})$, the quantity $|\bar{s}_i|^2$ satisfies $0 \leqslant |\bar{s}_i|^2 \leqslant r_{\max}^2$.

Generalizing the definition of weighted nearest-neighbor degree from Ref. [4] to networks with complex edge weights yields

$$k_{\mathrm{nn},i}^{w} = \frac{1}{s_i}\sum_{j=1}^{N} w_{ij}k_j\,. \tag{19}$$

One can separately track real and imaginary nearest-neighbor degrees by calculating $\mathrm{Re}(k_{\mathrm{nn},i}^{w})$ and $\mathrm{Im}(k_{\mathrm{nn},i}^{w})$.

In a binary and undirected network, the local clustering coefficient [124] of node i is

$$c_i = \frac{1}{k_i(k_i-1)}\sum_{j,k} a_{ij}a_{jk}a_{ki} \tag{20}$$

when $k_i \geqslant 2$. For $k_i = 0$ and $k_i = 1$, we set $c_i = 0$. There are a variety of ways to define local clustering coefficients in weighted networks [4,7,8]. Drawing inspiration from Ref. [7], we define the local weighted clustering coefficient of an undirected network with complex weights as

$$c_i^{\mathrm{w}} = \frac{1}{k_i(k_i-1)}\sum_{j,k}(\tilde{w}_{ij}\tilde{w}_{jk}\tilde{w}_{ki})^{1/3}\,, \tag{21}$$

where $\tilde{w}_{ij} = w_{ij}/\max_{i,j}|w_{ij}|$ is the normalized weight of the edge between nodes i and j. We also use Eq. (21) for directed networks in which the in-degree of each node is equal to its out-degree. [For more general directed networks, it is necessary to further generalize Eq. (21).] For $w_{ij} = ra_{ij}$ with $r > 0$, this weighted clustering coefficient equals the unweighted clustering coefficient c_i.

Instead of counting all triangles (i.e., closed triads, in which all possible edges are present) that are associated with a certain node in the same way, the weighted clustering coefficient c_i^{w} accounts for differences in the edge weights. For example, if a triangle connects nodes i, j, and k, then the unweighted local clustering coefficient counts the corresponding edges while ignoring their weights. However, if all of the normalized weights $\tilde{w}_{ij}$ that are associated with that triangle are close to 0, one may wish to weight the triangle differently than other (more important) triangles with larger edge weights. In networks with complex weights, it is possible to account not only for positive and negative edges (which arise, e.g., in correlation networks [125,126] and in subjects such as international relations [127,128]), but also to quantify directional and phase information (in addition to magnitudes). In Fig. 3(a), we show an example of a closed and undirected triad with edge weights $e^{\mathrm{i}\varphi}$. The local weighted clustering coefficient of node i is $c_i^{\mathrm{w}} = e^{\mathrm{i}\varphi}$. In the triad in Fig. 3(b), we use the edge weights $e^{\pm\mathrm{i}\varphi}$ to encode directional information. The corresponding local weighted clustering coefficient of node i is $c_i^{\mathrm{w}} = \cos(\varphi)$. This example illustrates that one can use the weighted clustering coefficient c_i^{w} to characterize the local arrangement of complex edge weights. If all weights have the same magnitude but the phases that are associated with the two cycles $i \to j \to k \to i$ and $i \to k \to j \to i$ have opposite signs, then the imaginary part of c_i^{w} is 0.

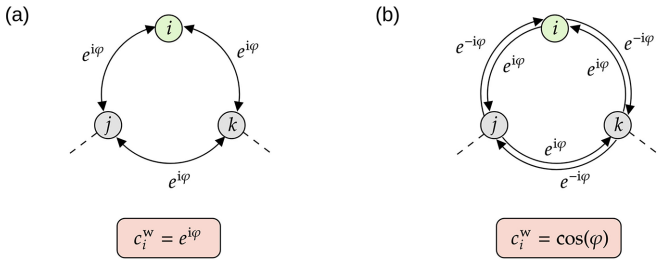

FIG. 3. Examples of clustering coefficients in a network with complex edge weights. (a) A closed and directed triad with complex weights $e^{\mathrm{i}\varphi}$. The weighted clustering coefficient of node i (in green) is $c_i^{\mathrm{w}} = e^{\mathrm{i}\varphi}$. (b) A closed and directed triad with complex weights $e^{\pm\mathrm{i}\varphi}$. The weighted clustering coefficient of node i (in green) is $c_i^{\mathrm{w}} = \cos(\varphi)$.

IV. MATRIX POWERS AND WALKS

Given an adjacency matrix A, the entries $a_{ij}^{(k)}$ of the matrix powers A^k (with $k \in \{1, 2, \ldots\}$) correspond to the number of walks of length k that start at node i and end at node j [129]. For a weight matrix W, the entry $w_{ij}^{(k)}$ of the matrix power W^k is equal to the sum of the products of all weights that are associated with each length-k walk from node i to node j. If W is a right-stochastic matrix, the entries of W^k correspond to the probabilities of reaching certain nodes from other nodes.

One advantage of complex-valued weights over real-valued weights is that using complex values allows one to encode directional information. Consider the network in Fig. 1(b). Clockwise and counterclockwise walks on this network have negative and positives phases, respectively. One can determine the "direction" of a walk on such a network from the accumulated phase of the product of the weights of the edges that a walker traverses. For example, the walks $1 \to 2 \to 1$ and $1 \to 2 \to 3$ have weight products of $e^{\mathrm{i}0}$ and $e^{\mathrm{i}2\pi/3}$, respectively. Therefore, their phases 0 and $2\pi/3$ indicate that the first walker traverses edges of opposite phase and returns to its initial position and that the second walker moves counterclockwise. In a quantum picture, one can interpret the positive and negative phases that are associated with a walk from i to j as Aharonov–Bohm phases that result from interactions between a charged particle and a magnetic vector potential $\mathbf{A}$ [34,83]. That is,

$$\varphi_{ij} = \int_{\mathcal{C}_{ij}} \mathbf{A}\cdot d\mathbf{x}\,, \tag{22}$$

where $\varphi_{ij} = -\varphi_{ji}$ and $\mathcal{C}_{ij}$ is a curve that starts at position $\mathbf{x}_i$ and ends at position $\mathbf{x}_j$. The amplitude r_{ij} in $w_{ij} = r_{ij}e^{\mathrm{i}\varphi_{ij}}$ is equal to a_{ij}. That is, $r_{ij} = 1$ if the charged particle can move from $\mathbf{x}_i$ to $\mathbf{x}_j$ and $r_{ij} = 0$ if it cannot. The resulting weight matrix is a discrete version of the magnetic Laplacian [34].

The complex edge weights $w_{ij} = e^{i\pi/3} = (1 + i\sqrt{3})/2$ and $w_{ji} = \bar{w}_{ij} = e^{-i\pi/3} = (1 - i\sqrt{3})/2$ in the triads in Fig. 1(b) have useful properties for applications in network analysis because both their product and their sum are equal to 1 (i.e., $w_{ij}w_{ji} = 1$ and $w_{ij} + w_{ji} = 1$) [68]. In the associated weight-matrix powers, a walk $i \to j \to i$ contributes 1 just as in the corresponding adjacency-matrix powers. As an example, we again consider the network in Fig. 1(b) and calculate the squares of its weight matrix W and adjacency matrix A. We obtain

$$W^2 = \begin{pmatrix} 2 & e^{-i2\pi/3} & e^{i2\pi/3} \\ e^{i2\pi/3} & 2 & e^{-i2\pi/3} \\ e^{-i2\pi/3} & e^{i2\pi/3} & 2 \end{pmatrix}, \quad A^2 = \begin{pmatrix} 2 & 1 & 1 \\ 1 & 2 & 1 \\ 1 & 1 & 2 \end{pmatrix}. \tag{23}$$

In this example, the diagonal entries of W^2 and A^2 are the same because of the multiplicative and additive properties of $e^{\pm i\pi/3}$.

Complex weights with fractional phases such as $\varphi = \pi/3$ arise in quantum-mechanical particle statistics. Exchanging bosonic particles in a multiparticle wave function is associated with the phase $\varphi = 0$, and exchanging fermions is associated with the phase $\varphi = \pi$. One can realize fractional phases $\varphi = \pi/(2m + 1)$ (with $m \in \mathbb{N}_{>0} = \{1, 2, \ldots\}$) that lie between those of bosons and fermions using anyons, which are quasiparticles that arise in 2D systems [97–101]. The phase $\varphi = \pi/3$ has been observed experimentally in anyon systems [100,101]. In a network that represents anyon permutations, one obtains the total phase that is associated with a permutation by multiplying the complex weights $e^{i\varphi_{ij}}$ in the $U(1)$ representation of the underlying braid group [130]. In an anyon system with exchange phase $\varphi = \pi/3$, exchanging two particles twice is associated with a total phase of $\varphi = 2\pi/3$, as one can see in some of the off-diagonal entries of W^2 in Eq. (23).

V. GRAPH ENERGY

The energy of a graph is

$$E(G) = \sum_{i=1}^{N} |\lambda_i|, \tag{24}$$

where λ_i is the ith eigenvalue of the weight matrix W [102]. To gain insight into the differences in the energy of binary networks, networks with real edge weights, and networks with complex edge weights, we compute graph energies for several well-studied types of networks.

In Hückel molecular-orbital (HMO) theory (i.e., tight-binding molecular-orbital theory), one typically represents conjugated hydrocarbon molecules by undirected and binary networks. The energy of π electrons in this HMO approximation is equivalent to the energy in Eq. (24) [102]. Although most applications of network analysis in mathematical chemistry have focused on undirected and binary molecular networks, weight matrices with real and complex entries have also been studied [38] (e.g., to examine cis and trans isomers of molecules [36,37]).

One can obtain closed-form expressions for the graph energy of certain graphs [102]. For example, the energy of almost every[3] $G(N, p)$ ER network [102,131] is

$$E[G(N, p)] = N^{3/2}\left(\frac{8}{3\pi}\sqrt{p(1-p)} + \mathcal{O}(1)\right), \tag{25}$$

where p is the connection probability and $f(x) = \mathcal{O}(1)$ means that $f(x)/c \to 0$ for any nonzero constant $c \in \mathbb{R}$. There are very few energy estimates for weighted networks, so in particular there are few such estimates for networks with complex edge weights [66]. We use graph energy to characterize ER, stochastic-block-model (SBM) [1], Watts–Strogatz (WS) [132], and Barabási–Albert (BA) [133] networks with binary, real, and complex weight distributions (see Fig. 4). We study one two-block SBM with community structure and one two-block SBM with core–periphery structure. In our calculations, we distribute the complex weights uniformly at random in the subset of the open unit disk in the first quadrant of the complex plane [i.e., $\varphi_{ij} \sim \mathcal{U}[0, \pi/2)$ and $r_{ij} = \sqrt{\epsilon_{ij}}$, where $\epsilon_{ij} \sim \mathcal{U}[0, 1)$ and $\mathcal{U}[a, b)$ denotes the uniform distribution on the half-open interval $[a, b)$] and distribute the real weights uniformly at random in the interval $[0, 4/3)$ [i.e., $w_{ij} \sim \mathcal{U}[0, 4/3)$]. We use the interval $[0, 4/3)$ to ensure that the mean value of the real weights is equal to the mean of the absolute value of the complex weights. The examined weight matrices are Hermitian. In Appendix B, we derive analogs of Eq. (25) for ER networks with these two weight distributions.

In Fig. 4, we show sample means of the graph energy $E(G)$ for ER, SBM, WS, and BA networks as a function of the parameters of these random-graph models. We show the corresponding eigenvalue distributions in Appendix B. For an ER network with binary edges [see Fig. 4(a)], the maximum of graph energy as $N \to \infty$ occurs when $p = 0.5$ [see Eq. (25)], whereas we observe that the examined real and complex weight distributions have graph-energy maxima when $p \approx 0.8$. The largest difference in graph energy between the examined ER networks with binary edges and their counterparts with real and complex edge weights occurs for $p = 1$ (i.e., in a fully connected graph). A binary ER network has a graph energy of $E[G(N, p = 1)] = 2(N - 1)$ (see Appendix C), whereas the corresponding weighted networks have larger values of graph energy for $N = 1000$ [see Fig. 4(a)] and presumably also as $N \to \infty$. The graph energies of the examined SBM networks, in which we vary only a single probability parameter, have similar qualitative behavior as the ER networks [see Figs. 4(b) and 4(c)]. For small interblock connection probabilities, one can approximate the graph energy of an SBM network that consists of ER blocks by the sum of the corresponding ER graph energies (25).

The mean graph energy of the WS networks is largely independent of the rewiring probability q. In the BA networks, the mean graph energy increases with m, which is the number of new edges that one adds for each new node. For the examined WS and BA networks, the mean graph energies that we obtain

[3] In the present paper, we say that "almost every" graph $\hat{G}$ in a random-graph model G with N nodes has a certain property if the probability that $\hat{G}$ satisfies that property approaches 1 as $N \to \infty$.

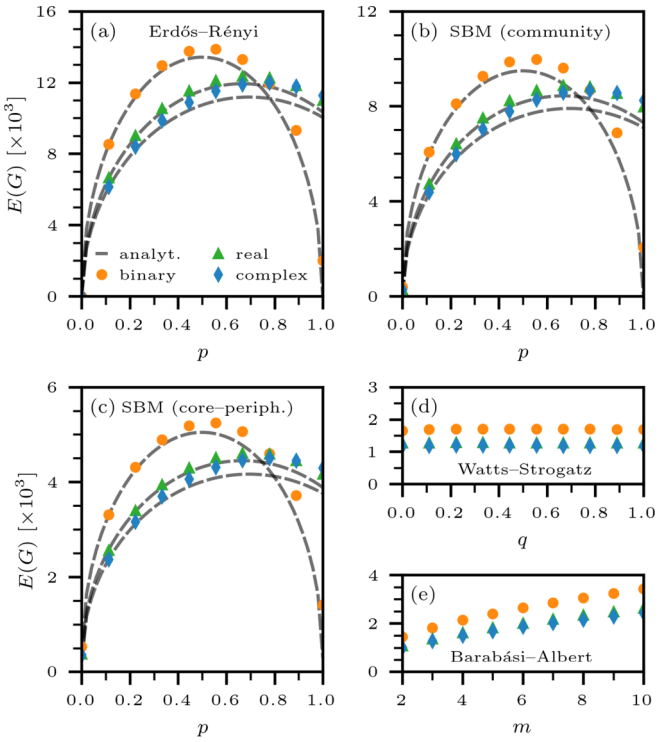

FIG. 4. Graph energies for different networks with binary, real, and complex edge weights. We show the graph energies $E(G)$ [see Eq. (24)] for five types of networks with binary, real, and complex weight distributions: (a) a $G(N, p)$ ER network, (b) a stochastic block model (SBM) with two $G(N, p)$ ER blocks and interblock connection probability 10^{-3}, (c) an SBM with one $G(N, p)$ ER block for general p, one $G(N, p)$ ER block with $p = 10^{-3}$, and interblock connection probability 10^{-3}, (d) a $G(N, k, q)$ Watts–Strogatz (WS) network in which each node is adjacent to $k = 4$ nearest neighbors (where q denotes the probability of rewiring each edge), and (e) a Barabási–Albert (BA) network. All of these networks have $N = 1000$ nodes. In all simulations that involve weighted networks, we use Hermitian weight matrices (i.e., $W = W^\dagger$). To construct the BA network, we start with a star graph with 1 hub and m leaves, and we iteratively add new nodes until there are 1000 nodes. Each new node has m edges that connect to existing nodes using linear preferential attachment. The orange disks indicate numerical results for binary weight matrices (i.e., for $W = A$). The green triangles indicate numerical results for networks with real-valued weight distributions, and the blue diamonds indicate numerical results for networks with complex-valued weight distributions. The real weights are distributed uniformly in the interval $[0, 4/3)$, and the complex weights are distributed uniformly in the subset of the open unit disk in the first quadrant of the complex plane. All reported results are means of 100 independent instantiations of the indicated random-graph models. For each instantiation, we use the same network structure, but we change the weights (which can be binary, real, or complex). The dashed gray curves in panels (a)–(c) are based on the analytical solutions (25), (B4), and (B5), which assume that $N \to \infty$.

for binary weights are larger than those for the examined real and complex weights. Although the mean values of the examined real weights equal the means of the absolute values of the associated complex weights, the mean values of $E(G)$ for the ER networks with real weights are larger than those of their counterparts with complex weights for $p \lessapprox 0.8$. For $p \gtrapprox 0.8$, the mean graph energy is larger for ER networks with complex weights than for ER networks with real or binary weights. In the WS and BA networks, the graph energies that we obtain with real weights are about 5% and 8% larger, respectively, than the energies that we obtain with complex weights.

In summary, graph energy is qualitatively different in binary networks, networks with real edge weights, and networks with complex edge weights. This is the case both for the magnitude of the graph energy and for how it depends on network connectivity properties (as quantified by the network parameters p, q, and m). Given the described connections between graph energy and energy estimates of conjugated molecules, our results may be relevant to the modeling of molecules with weighted networks.

VI. THE PERRON–FROBENIUS THEOREM AND EIGENVECTOR CENTRALITY

According to the Perron–Frobenius theorem [103,104], the weight matrix $W = A$ of a binary, strongly connected network is associated with a simple positive eigenvalue (the "Perron eigenvalue") that is strictly larger than all other eigenvalues. The Perron eigenvalue is equal to $\rho(W) = \max_{i\in\{1,\dots,N\}} |\lambda_i|$, the spectral radius of W, where $\{\lambda_i\}_{i\in\{1,\dots,N\}}$ is the set of eigenvalues (i.e., the spectrum) of W. The corresponding Perron eigenvector (i.e., the leading eigenvector) is a centrality measure [1].

The Perron–Frobenius theorem does not hold for matrices with complex weights, so we cannot find a Perron eigenvalue of W and a corresponding eigenvector to use as a centrality measure. However, generalizations of the Perron–Frobenius theorem [105,106] provide a possible approach to define eigenvector centrality (and generalizations of it, such as PageRank) for networks with certain types of complex weight matrices. A complex weight matrix W has the "strong Perron–Frobenius property" if it (1) has a simple positive eigenvalue λ_1 that satisfies $\lambda_1 = \rho(W) > |\lambda_i|$ (with $i \in \{2, \dots, N\}$) and (2) has a corresponding right eigenvector $\mathbf{v}_1$ with positive entries. The eigenvector $\mathbf{v}_1$ is called the "right Perron–Frobenius eigenvector". For further details about generalizations of the Perron–Frobenius theorem to complex matrices, see Ref. [106].

An example of a weight matrix with the strong Perron–Frobenius property is

$$W = \begin{pmatrix} 0 & ae^{\mathrm{i}\varphi_a} & 0 \\ be^{\mathrm{i}\varphi_b} & 0 & ce^{\mathrm{i}\varphi_c} \\ 0 & de^{\mathrm{i}\varphi_d} & 0 \end{pmatrix}, \tag{26}$$

with $a = b = c = 1$, $d = -1/2$, $\varphi_a = 0$, $\varphi_b = \pi/6$, $\varphi_c = 3\pi/2$, and $\varphi_d = \pi$. Inserting these parameter values gives

$$W = \begin{pmatrix} 0 & 1 & 0 \\ e^{\mathrm{i}\pi/6} & 0 & -\mathrm{i} \\ 0 & 1/2 & 0 \end{pmatrix}. \tag{27}$$

The largest eigenvalue of W is $\sqrt[4]{3/4}$, and its corresponding eigenvector is $\mathbf{v}_1 = (2, \sqrt[4]{12}, 1)^\top$. What is the meaning of the right Perron–Frobenius eigenvector $\mathbf{v}_1$ for the eigenvector centralities that are associated with a complex weight matrix?

In this example, nodes 1, 2, and 3 have eigenvector centralities of 2, $\sqrt[4]{12}$, and 1, respectively. The most central nodes of the associated network are thus nodes 1 and 2, whereas node 3 (which has a single out-edge with weight $1/2$) is the least central node. In this example, the eigenvector centralities that we obtain using the complex weight matrix W coincide with the eigenvector centralities that we obtain using $\mathrm{Re}(W)$.

In Appendix D, we show that any Hermitian two-node network with complex edges weights with nonzero imaginary parts cannot satisfy the strong Perron–Frobenius property.

VII. BETWEENNESS AND CLOSENESS CENTRALITIES

The geodesic betweenness centrality $c_{\mathrm{B}}(i)$ of a node i quantifies the number of shortest paths that traverse that node, and the closeness centrality $c(i)$ of a node i quantifies the mean distance between that node and other nodes [1]. Mathematically, the normalized geodesic betweenness centrality of node i in a directed network is

$$c_{\mathrm{B}}(i) = \frac{1}{(N-1)(N-2)} \sum_{\{j,k|j\neq i,k\neq i\}} \frac{\sigma_{jk}(i)}{\sigma_{jk}}, \qquad (28)$$

where the numerator σ_{jk} is the total number of shortest paths between nodes j and k and the denominator $\sigma_{jk}(i)$ is the number of those shortest paths that traverse node i. The closeness centrality of node i is

$$c(i) = \frac{N-1}{\sum_{j\neq i} d_{ij}}, \qquad (29)$$

where d_{ij} is the geodesic (i.e., shortest-path) distance between nodes i and j.

Because complex numbers are not fully ordered, one cannot use geodesic betweenness and closeness centrality measures that are based on shortest paths on networks with complex weights. Except in degenerate situations, one cannot order path lengths in networks with complex edge weights. As in the above examples for occupation and eigenvector centralities (see Secs. II and VI), one has to appropriately generalize geodesic betweenness and closeness centralities. One way to quantify node importances in a network with a complex weight matrix is to use quantum random-walk centrality measures [28]. In Eq. (5), we presented an occupation-centrality measure that is based on a quantum random walk with Hamiltonian $H_{\mathrm{q}} = -W$ and Hermitian W. In Appendix E, we describe corresponding generalizations of betweenness and closeness that are based on absorbing random walks and can take complex weight matrices as inputs.

We first apply these centrality measures to a network with three nodes (see Fig. 5) and weight matrix

$$W = \begin{pmatrix} 0 & e^{\mathrm{i}\varphi} & e^{\mathrm{i}\varphi} \\ e^{-\mathrm{i}\varphi} & 0 & 0 \\ e^{-\mathrm{i}\varphi} & 0 & 0 \end{pmatrix}. \qquad (30)$$

In the associated unweighted (i.e., binary) analog of this network, the geodesic betweenness centralities of nodes 1, 2, and 3 are 1, 0, and 0, respectively. The corresponding quantum random-walk betweenness centralities that are associated with the Hamiltonian $H_{\mathrm{q}} = -W$ with $\varphi = \pi/3$ are 1, 0.65, and 0.65. (We normalize the betweenness values so that the maximum is 1.) The ranking of the nodes is the same for geodesic betweenness centrality. To calculate a quantum random-walk version of closeness centrality (see Appendix E), we first calculate the mean return time (i.e., the inverse of the occupation probability). We calculate quantum random-walk occupation centrality π_j (with $j \in \{1, 2, 3\}$) by evaluating the infinite-time mean (5), where $|\psi(t)\rangle = e^{-\mathrm{i}H_{\mathrm{q}}t}|\psi(0)\rangle$. We set $|\psi(0)\rangle = (1, 1, 1)^{\top}/\sqrt{3}$ and find that the infinite-time mean is $\boldsymbol{\pi} = (0.5, 0.25, 0.25)^{\top}$. In this example, the occupation centrality of node 1 is twice as large as those of nodes 2 and 3. The corresponding quantum random-walk closeness values are 1, 0.9, and 0.9. (We normalize these values so that the maximum is 1.) As we saw with betweenness centrality, quantum random-walk closeness yields the same node ranking as geodesic closeness.

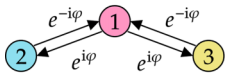

	node		
	1	**2**	**3**
betweenness	1	0	0
closeness	1	2/3	2/3

FIG. 5. Betweenness and closeness centralities of a network with three nodes and the weight matrix (30). In the table, we show the geodesic betweenness and closeness centralities of nodes 1, 2, and 3 that are associated with the unweighted (i.e., binary) analog of the depicted network.

We now compare geodesic and quantum random-walk centralities for ER and BA networks with $N = 1000$ nodes and complex edge weights that (as in our examination of graph energy) we distribute uniformly at random in the subset of the open unit disk in the first quadrant of the complex plane. We again consider the evolution operator $H_{\mathrm{q}} = -W$ [see Eq. (4)]. In Fig. 6, we show scatter plots to compare the geodesic and quantum random-walk centralities. In the examined ER and BA networks, both betweenness and closeness have Pearson correlation coefficients that range from 0.36 to 1.00. Our results suggest that quantum random-walk closeness and betweenness centralities are able to rank node importances in networks with complex weights in a manner that is similar to their corresponding geodesic centralities.

VIII. CONCLUSIONS AND DISCUSSION

Networks with complex-valued edge weights arise in a variety of situations. However, most studies of weighted networks have focused on networks with real-valued edge weights.

In the present paper, we examined network-analysis methods that are useful to study the structure of networks with complex edge weights. To physically interpret such networks and the underlying directional information that is encoded in the phases of the complex weights, we discussed connections between complex weight matrices and salient physical systems. For example, perhaps the phases that are associated with a walk on a network with complex edge weights arise from interactions between a charged particle (which traverses the edges) and a vector potential. Moreover, akin to the interpretation of stochastic weight matrices as generators of linear

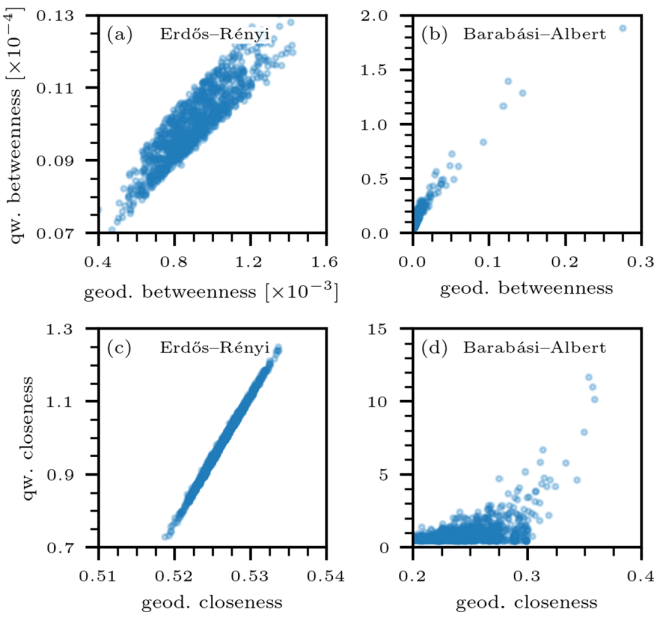

FIG. 6. Quantum random-walk versus geodesic betweenness and closeness centralities. We illustrate the correlations between quantum random-walk (qw) and geodesic centralities for (a, b) betweenness and (c, d) closeness. In panels (a) and (c), we show scatter plots for a $G(N, p)$ ER network with $p = 0.1$. In panels (b) and (d), we show scatter plots for a BA network that we construct from an initial star graph with 1 hub and 2 leaves by iteratively adding new nodes until there are $N = 1000$ nodes. Each new node has $m = 2$ edges that connect to existing nodes using linear preferential attachment. Both networks have 1000 nodes. The Pearson correlation coefficients are (a) 0.89, (b) 0.81, (c) 1.00, and (d) 0.36. We calculate the geodesic centralities for binary networks. To calculate the quantum random-walk centralities, we use $H_{\mathrm{q}} = -W$ [see Eq. (4)] as the evolution operator. We suppose that W is Hermitian, so $W = W^{\dagger}$. Aside from the Hermiticity constraint, we distribute the weights uniformly at random in the subset of the open unit disk in the first quadrant of the complex plane.

diffusion dynamics (i.e., random walks), we showed that one can interpret Hermitian weight matrices with complex entries as generators of time translation in continuous-time quantum walks. We also generalized the DeGroot model of consensus dynamics to networks with complex edge weights. Finally, we characterized the structural features of networks with complex edge weights using a variety of measures (specifically, graph energy, common centrality measures, and generalizations of node strength and a local clustering coefficient).

Given the diverse variety of applications of networks with complex weights (see Table I), there are many interesting directions for future work. We mention a few of them in passing. A recent paper examined random walks and structural balance in networks with complex edge weights [50], and there are many exciting directions to pursue to build on it. Another potentially valuable area is investigating the properties of electrical networks of resistors, coils, and capacitors [41–47] using network analysis. In such networks, one can use complex weights to describe complex impedances and reflection coefficients. Another avenue for future research is analytical investigations of graph energy in networks with both real and complex weights. Such efforts can build fruitfully on random-matrix-theory analyses of weighted networks [134]. Furthermore, given the importance of the Perron–Frobenius theorem for dynamical processes and centrality measures in networks with real weights, it is worthwhile to identify physical systems with associated complex weight matrices that satisfy the strong Perron-Frobenius property. Studies of such systems may help further guide the development of suitable centralities, spectral clustering methods [135], and other network measures to study physical systems with complex weight matrices. Additionally, given the relevance of motifs in the study of both unweighted and weighted networks, it seems worthwhile to examine motifs in networks with complex edge weights, such as by generalizing walk-based motifs from classical contexts [136] to quantum ones.

Our code is publicly available at [110].

ACKNOWLEDGMENTS

We thank Ginestra Bianconi, Tom Burns, Lincoln Carr, Karen Daniels, Ernesto Estrada, Alexander Goltsev, Malte Henkel, Adam Knapp, Renaud Lambiotte, Cris Moore, Matteo Paris, and three anonymous referees for helpful comments.

APPENDIX A: QUANTUM SYNCHRONIZATION

The quantum-state evolution (8) conserves the L_2 norm that is associated with $|\psi_i\rangle$. That is, $\partial_t \|\psi_i\|^2 = \langle \partial_t \psi_i | \psi_i \rangle + \langle \psi_i | \partial_t \psi_i \rangle = 0$ because

$$\langle \psi_i | \partial_t \psi_i \rangle = \sum_{j=1}^{N} a_{ij} [\langle \psi_i | \psi_j \rangle - \langle \psi_j | \psi_i \rangle] ,$$
$$\langle \partial_t \psi_i | \psi_i \rangle = \sum_{j=1}^{N} a_{ij} [\langle \psi_j | \psi_i \rangle - \langle \psi_i | \psi_j \rangle] . \tag{A1}$$

APPENDIX B: EIGENVALUE DISTRIBUTIONS

In Fig. 7, we show the eigenvalue distributions of W for the networks that we studied in Sec. V. The analytical results in Fig. 7(a) (see the solid gray curves) are based on a connection between the examined weight matrices and Wigner matrices [137]. A Wigner matrix X_N is a real symmetric matrix with entries x_{ij} (with $i, j \in \{1, \ldots, N\}$) that have the following properties [102]:

(1) The entries x_{ij} are independent random variables with $x_{ij} = x_{ji}$.

(2) The diagonal entries x_{ii} are distributed according to a distribution F_1, and the off-diagonal entries x_{ij} (with $i \neq j$) are distributed according to a distribution F_2.

(3) The distribution F_2 has finite variance $\mathrm{Var}(x_{ij}) = \sigma_2^2 < \infty$.

As $N \to \infty$, the eigenvalue distribution of a normalized Wigner matrix X_N/N converges almost surely to the Wigner semicircle distribution

$$\phi(x) = \frac{1}{2\pi\sigma_2^2} \sqrt{4\sigma_2^2 - x^2}\, \mathbf{1}_{|x|<2\sigma_2} , \tag{B1}$$

where $\mathbf{1}_S$ denotes the indicator function on the set S.

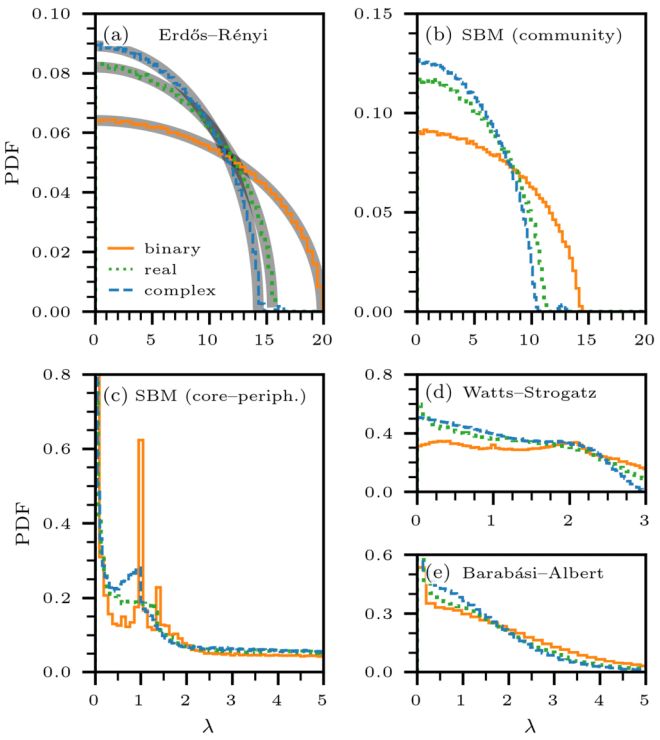

FIG. 7. Eigenvalue distributions for different networks with binary, real, and complex edge weights. We show the eigenvalue distributions for five types of networks with binary, real, and complex weight distributions: (a) a $G(N, p)$ ER network with $p = 1/9$ (where p is the connection probability), (b) an SBM with two $G(N, p)$ ER blocks with $p = 1/9$ and interblock connection probability 10^{-3}, (c) an SBM with one $G(N, p)$ ER block with $p = 1/9$, one $G(N, p)$ ER block with $p = 10^{-3}$, and interblock connection probability 10^{-3}, (d) a $G(N, k, q)$ WS network in which $q = 1/9$ and each node is adjacent to $k = 4$ nearest neighbors (where q is the probability of rewiring each edge), and (e) a BA network. All of these networks have $N = 1000$ nodes. In all simulations with weighted networks, we use Hermitian weight matrices (i.e., $W = W^\dagger$). To construct the BA network, we start with a star graph with 1 hub and 2 leaves and iteratively add new nodes until there are $N = 1000$ nodes. Each new node has $m = 2$ edges that connect to existing nodes using linear preferential attachment. The solid orange curves indicate numerical results for binary weight matrices (i.e., for $W = A$). The dotted green curves indicate numerical results for real-valued weight distributions, and the dashed blue curves indicate numerical results for networks with complex-valued weight distributions. We distribute the real weights uniformly at random in the interval $[0, 4/3)$, and we distribute the complex weights uniformly at random in the subset of the open unit disk in the first quadrant of the complex plane. Each result is a mean of 100 independent instantiations of the indicated random-graph models. For each instantiation, we use the same network structure, but we change the weights (which can be binary, real, or complex). The solid gray curves in panel (a) indicate the analytical solution (B1) for $\sigma_2^2 = p(1-p)$, $\sigma_2^2 = 4(4-3p)p/27$, and $\sigma_2^2 = p/2 - 32p^2/(9\pi^2)$ [see Eqs. (B3)–(B5)].

For the $G(N, p)$ ER random-graph model with binary edge weights, the variance is $\sigma_2^2 = p(1-p)$, which yields the $\sqrt{p(1-p)}$ term in Eq. (25).

The weights w_{ij} (with $i \neq j$) of the $G(N, p)$ ER networks with real-valued weight matrices that we studied in Sec. V are

$$w_{ij} = w_{ji} = \begin{cases} x_{ij}\,, & \text{with probability } p \\ 0\,, & \text{with probability } 1-p\,, \end{cases} \tag{B2}$$

where $x_{ij} \sim \mathcal{U}[a, b)$ and $\mathcal{U}[a, b)$ denotes the uniform distribution on the interval $[a, b)$. The corresponding variance is

$$\begin{aligned} \sigma_2^2 &= \frac{p}{b-a}\int_a^b x^2 dx - \frac{p^2(a+b)^2}{4} \\ &= \frac{1}{12}p[4(a^2+ab+b^2) - 3(a+b)^2 p]\,. \end{aligned} \tag{B3}$$

For $x_{ij} \sim \mathcal{U}[0, 4/3)$ (with $i \neq j$), the energy of almost every $G(N, p)$ ER network with real-valued weights (see Sec. V) is

$$E[G(N,p)] = N^{3/2}\left(\frac{8}{3\pi}\sqrt{\frac{4(4-3p)p}{27}} + \mathcal{O}(1)\right). \tag{B4}$$

For a $G(N, p)$ ER network with complex-valued weights, a similar calculation yields

$$E[G(N,p)] = N^{3/2}\left(\frac{8}{3\pi}\sqrt{\frac{p}{2} - \frac{32p^2}{9\pi^2}} + \mathcal{O}(1)\right), \tag{B5}$$

which we obtain using the relations $\mathrm{Var}(Z) = \mathrm{Var}(\mathrm{Re}(Z)) + \mathrm{Var}(\mathrm{Im}(Z))$ and $\mathrm{Var}(XY) = (\sigma_X^2 + \mu_X^2)(\sigma_Y^2 + \mu_Y^2) - \mu_X^2\mu_Y^2$, where μ_X and σ_X^2 denote the mean and variance of the random variable X. Initially, Wigner derived the semicircle law (B1) for real symmetric matrices [137]. Subsequently, researchers have examined generalizations to complex-valued Hermitian matrices (see, e.g., Ref. [138]).

APPENDIX C: ERDŐS–RÉNYI GRAPH ENERGY WITH $p = 1$

As $p \to 1$, a binary $G(N, p)$ Erdős-Rényi (ER) network approaches a complete graph, which has the adjacency matrix

$$A = \mathbf{u}\mathbf{u}^\top - \mathbb{1}\,, \tag{C1}$$

where $\mathbf{u} \in \mathbb{R}^N$ denotes a vector whose entries are all equal to 1 and $\mathbb{1}$ denotes the $N \times N$ identity matrix. We calculate the eigenvalues of A by distinguishing two cases of the eigenvalue equation $A\mathbf{v} = \langle \mathbf{u}, \mathbf{v}\rangle \mathbf{u} - \mathbf{v} = \lambda \mathbf{v}$. For the $N-1$ eigenvectors that are orthogonal to $\mathbf{u}$, we have $\langle \mathbf{u}, \mathbf{v}\rangle = 0$. The corresponding eigenvalue (of multiplicity $N-1$) is -1. The remaining eigenvector $\mathbf{v} = \mathbf{u}$ is associated with the eigenvalue $N-1$.

As $p \to 1$, the energy of a binary $G(N, p)$ ER network approaches the energy of a complete graph, which is

$$\sum_{i=1}^{N} |\lambda_i| = 2(N-1)\,. \tag{C2}$$

APPENDIX D: ABSENCE OF THE STRONG PERRON–FROBENIUS PROPERTY IN HERMITIAN TWO-NODE NETWORKS WITH COMPLEX EDGE WEIGHTS WITH NONZERO IMAGINARY PARTS

Consider a two-node network with complex edge weights and the Hermitian weight matrix

$$W = \begin{pmatrix} a & be^{\mathrm{i}\varphi} \\ be^{-\mathrm{i}\varphi} & c \end{pmatrix}, \tag{D1}$$

where $a, b, c \in \mathbb{R}_{\geqslant 0}$ and $\varphi \in [0, 2\pi)$. Equation (D1) allows self-weights. The largest eigenvalue of W is

$$\tfrac{1}{2}(a + c\sqrt{(a-c)^2 + 4b^2}), \tag{D2}$$

and the corresponding eigenvector is

$$\left(\frac{e^{\mathrm{i}\varphi}(a - c + \sqrt{(a-c)^2 + 4b^2})}{2b}, 1\right)^{\top}. \tag{D3}$$

The imaginary part of the off-diagonal components of W is 0 for $\varphi = 0$ and $\varphi = \pi$. However, for the eigenvector (D3) to be positive, the phase φ must be either 0 or π. Therefore, the imaginary parts of the off-diagonal entries of W [see Eq. (D1)] are 0. Consequently, it is not possible for a two-node network with a Hermitian weight matrix to have off-diagonal matrix entries with nonzero imaginary parts and also satisfy the strong Perron–Frobenius property [106].

APPENDIX E: QUANTUM RANDOM-WALK BETWEENNESS AND CLOSENESS CENTRALITIES

In Section II A, we used the infinite-time mean (5) of a CTQW [see Eq. (4)] to define the occupation centralities of the nodes of a network with a Hermitian weight matrix W. To characterize the betweenness and closeness centralities of the nodes of a network with complex weights, we first define the absorbing quantum random-walk Hamiltonian

$$\left[(H_\ell)^{\mathrm{a}}_{\mathrm{q}}\right]_{ij} = \begin{cases} (H_{\mathrm{q}})_{ij}\,, & \text{if } j \neq \ell \\ 0\,, & \text{if } j = \ell\,, \end{cases} \tag{E1}$$

with absorbing node ℓ. The basic idea that underlies the use of an absorbing Hamiltonian is that we wish to track the number of times that a quantum random walker traverses a node if its final destination is ℓ [28,109]. Taking a mean over all absorbing nodes yields a measure of random-walk betweenness centrality. The operator $(H_\ell)^{\mathrm{a}}_{\mathrm{q}}$ is non-Hermitian. To evaluate its infinite-time mean (5), we treat the upper-triangular part of $(H_\ell)^{\mathrm{a}}_{\mathrm{q}}$ as equal to the conjugate transpose of its lower-triangular part. To do so, we use eigenvalue-problem solvers such as `scipy.linalg.eigh` (SCIPY version 1.9.1) and `numpy.linalg.eigh` (NUMPY version 1.23), which treat non-Hermitian matrices as Hermitian matrices. We denote the corresponding Hermitian version of $(H_\ell)^{\mathrm{a}}_{\mathrm{q}}$ by $(\widetilde{H}_\ell)^{\mathrm{a}}_{\mathrm{q}}$.

The quantum random-walk betweenness centrality of node j is

$$\tau_j = \lim_{s\to 0} \frac{1}{N(N-1)} \sum_{\ell} \sum_{m,n} \frac{\langle e_m^{(\ell)} | \psi(0)\rangle \langle \psi(0) | e_n^{(\ell)}\rangle}{s + \mathrm{i}\left(\lambda_m^{(\ell)} - \lambda_n^{(\ell)}\right)} \times \langle j | e_m^{(\ell)}\rangle \langle e_n^{(\ell)} | j\rangle\,, \tag{E2}$$

where $|\psi(0)\rangle = (1, \ldots, 1)^{\top}/\sqrt{N}$ and $e_m^{(\ell)}$ and $\lambda_m^{(\ell)}$, respectively, are the orthonormal eigenvectors and corresponding eigenvalues of the Hamiltonian $(\widetilde{H}_\ell)^{\mathrm{a}}_{\mathrm{q}}$ [28]. That is,

$$(\widetilde{H}_\ell)^{\mathrm{a}}_{\mathrm{q}} e_m^{(\ell)} = \lambda_m^{(\ell)} e_m^{(\ell)}\,, \quad \langle e_m^{(\ell)} | e_n^{(\ell)}\rangle = \delta_{mn}\,. \tag{E3}$$

We use the regularization parameter s in Eq. (E2) to prevent the denominator from equaling 0 when $\lambda_m^{(\ell)} = \lambda_n^{(\ell)}$. In all of our numerical experiments, we set $s = 10^{-1}$.

The quantum random-walk closeness centrality of node ℓ is equal to the inverse of the mean first-passage time h_ℓ of a walker that starts at any node and stops when it arrives at node ℓ. The mean first-passage time is

$$h_\ell = \frac{1}{N-1} \sum_{i,j} (\tau_\ell)_{ij} + \frac{1}{N} \pi_\ell^{-1}\,, \tag{E4}$$

where $(\tau_\ell)_{ij}$ denotes the expected number of times that a random walker that starts at node i with final destination ℓ traverses node j at any time. As in Eq. (E2), we do not sum over all initial nodes i; instead, we consider a uniform initial walker state $|\psi(0)\rangle = (1, \ldots, 1)^{\top}/\sqrt{N}$ and compute $\sum_j (\tau_\ell)_j$ in terms of Eq. (E2) by replacing the sum over ℓ with a sum over j. The quantity π_ℓ^{-1} is the inverse of the occupation probability (5) (i.e., the mean return time).

For more information about classical and quantum random-walk centrality measures and their generalizations to multilayer networks, see Refs. [28,109].

[1] M. E. J. Newman, *Networks*, 2nd ed. (Oxford University Press, Oxford, UK, 2018).

[2] M. A. Porter and J. P. Gleeson, *Dynamical Systems on Networks: A Tutorial*, Frontiers in Applied Dynamical Systems: Reviews and Tutorials (Springer International Publishing, Cham, Switzerland, 2016), Vol. 4.

[3] M. Salathé, M. Kazandjieva, J. W. Lee, P. Levis, M. W. Feldman, and J. H. Jones, A high-resolution human contact network for infectious disease transmission, Proc. Natl. Acad. Sci. USA **107**, 22020 (2010).

[4] A. Barrat, M. Barthelemy, R. Pastor-Satorras, and A. Vespignani, The architecture of complex weighted networks, Proc. Natl. Acad. Sci. USA **101**, 3747 (2004).

[5] A. A. S. T. Ribeiro and V. Ortiz, Determination of signaling pathways in proteins through network theory: Importance of the topology, J. Chem. Theory Comput. **10**, 1762 (2014).

[6] M. E. J. Newman, Analysis of weighted networks, Phys. Rev. E **70**, 056131 (2004).

[7] J.-P. Onnela, J. Saramäki, J. Kertész, and K. Kaski, Intensity and coherence of motifs in weighted complex networks, Phys. Rev. E **71**, 065103(R) (2005).

[8] J. Saramäki, M. Kivelä, J.-P. Onnela, K. Kaski, and J. Kertész, Generalizations of the clustering coefficient to weighted complex networks, Phys. Rev. E **75**, 027105 (2007).

[9] S. Horvath, *Weighted Network Analysis: Applications in Genomics and Systems Biology* (Springer-Verlag, Heidelberg, Germany, 2011).

[10] G. J. Li and M. A. Porter, Bounded-confidence model of opinion dynamics with heterogeneous node-activity levels, Phys. Rev. Res. **5**, 023179 (2023).

[11] W. Heisenberg, Über quantentheoretische Umdeutung kinematischer und mechanischer Beziehungen, Eur. Phys. J. A **33**, 879 (1925).

[12] E. Schrödinger, Quantisierung als Eigenwertproblem, Ann. Phys. (Berlin, Ger.) **386**, 109 (1926).

[13] P. A. M. Dirac, *The Principles of Quantum Mechanics* (Oxford University Press, Oxford, UK, 1930).

[14] M. McKague, M. Mosca, and N. Gisin, Simulating quantum systems using real Hilbert spaces, Phys. Rev. Lett. **102**, 020505 (2009).

[15] M.-O. Renou, D. Trillo, M. Weilenmann, T. P. Le, A. Tavakoli, N. Gisin, A. Acín, and M. Navascués, Quantum theory based on real numbers can be experimentally falsified, Nature **600**, 625 (2021).

[16] M.-C. Chen, C. Wang, F.-M. Liu, J.-W. Wang, C. Ying, Z.-X. Shang, Y. Wu, M. Gong, H. Deng, F.-T. Liang, Q. Zhang, C.-Z. Peng, X. Zhu, A. Cabello, C.-Y. Lu, and J.-W. Pan, Ruling out real-valued standard formalism of quantum theory, Phys. Rev. Lett. **128**, 040403 (2022).

[17] Z.-D. Li, Y.-L. Mao, M. Weilenmann, A. Tavakoli, H. Chen, L. Feng, S.-J. Yang, M.-O. Renou, D. Trillo, T. P. Le, N. Gisin, A. Acín, M. Navascués, Z. Wang, and J. Fan, Testing real quantum theory in an optical quantum network, Phys. Rev. Lett. **128**, 040402 (2022).

[18] D. P. Reichert and T. Serre, Neuronal synchrony in complex-valued deep networks, in *2nd International Conference on Learning Representations, ICLR 2014, Banff, Alberta, Canada, April 14–16, 2014, Conference Track Proceedings*, edited by Y. Bengio and Y. Le Cun (ICLR, 2014).

[19] A. Hirose, *Complex-Valued Neural Networks* (Springer-Verlag, Heidelberg, Germany, 2012).

[20] C. Lee, H. Hasegawa, and S. Gao, Complex-valued neural networks: A comprehensive survey, IEEE/CAA J. Autom. Sin. **9**, 1406 (2022).

[21] I. Nemoto and K. Saito, A complex-valued version of Nagumo–Sato model of a single neuron and its behavior, Neural Netw. **15**, 833 (2002).

[22] F. Gomez, T. Lorimer, and R. Stoop, Signal-coupled subthreshold Hopf-type systems show a sharpened collective response, Phys. Rev. Lett. **116**, 108101 (2016).

[23] A. M. Childs, E. Farhi, and S. Gutmann, An example of the difference between quantum and classical random walks, Quantum Inf. Process. **1**, 35 (2002).

[24] C. Moore and A. Russell, Quantum walks on the hypercube, in *Randomization and Approximation Techniques in Computer Science: 6th International Workshop, RANDOM 2002 Cambridge, MA, USA, September 13–15, 2002, Proceedings*, edited by J. D. P. Rolim and S. Vadhan (Springer-Verlag, Heidelberg, Germany, 2002), pp. 164–178.

[25] A. M. Childs and J. Goldstone, Spatial search by quantum walk, Phys. Rev. A **70**, 022314 (2004).

[26] O. Mülken and A. Blumen, Continuous-time quantum walks: Models for coherent transport on complex networks, Phys. Rep. **502**, 37 (2011).

[27] R. Portugal, *Quantum Walks and Search Algorithms* (Springer-Verlag, Heidelberg, Germany, 2013).

[28] L. Böttcher and M. A. Porter, Classical and quantum random-walk centrality measures in multilayer networks, SIAM J. Appl. Math. **81**, 2704 (2021).

[29] S. Kubota, E. Segawa, and T. Taniguchi, Quantum walks defined by digraphs and generalized Hermitian adjacency matrices, Quantum Inf. Process. **20**, 95 (2021).

[30] K. Kadian, S. Garhwal, and A. Kumar, Quantum walk and its application domains: A systematic review, Comput. Sci. Rev. **41**, 100419 (2021).

[31] M. Frigerio, C. Benedetti, S. Olivares, and M. G. A. Paris, Generalized quantum-classical correspondence for random walks on graphs, Phys. Rev. A **104**, L030201 (2021).

[32] C.-H. Wu and G. Mahler, Quantum network theory of transport with application to the generalized Aharonov–Bohm effect in metals and semiconductors, Phys. Rev. B **43**, 5012 (1991).

[33] Y. Liu, Z. Hou, P. M. Hui, and W. Sritrakool, Electronic transport properties of Sierpinski lattices, Phys. Rev. B **60**, 13444 (1999).

[34] E. H. Lieb and M. Loss, Fluxes, Laplacians, and Kasteleyn's theorem, Duke Math. J. **71**, 337 (1993).

[35] P. Vasilopoulos, O. Kálmán, F. M. Peeters, and M. G. Benedict, Aharonov–Bohm oscillations in a mesoscopic ring with asymmetric arm-dependent injection, Phys. Rev. B **75**, 035304 (2007).

[36] G. Lekishvili, On the characterization of molecular stereostructure: 1. Cis–trans isomerism, J. Chem. Inf. Comput. Sci. **37**, 924 (1997).

[37] A. Golbraikh, D. Bonchev, and A. Tropsha, Novel *ZE*-isomerism descriptors derived from molecular topology and their application to QSAR analysis, J. Chem. Inf. Comput. Sci. **42**, 769 (2002).

[38] E. Estrada, J. A. Rodríguez-Velázquez, and M. Randić, Atomic branching in molecules, Int. J. Quantum Chem. **106**, 823 (2006).

[39] C. R. Paul, *Analysis of Multiconductor Transmission Lines* (John Wiley & Sons, Hoboken, NJ, USA, 2007).

[40] S. H. Strub and L. Böttcher, Modeling deformed transmission lines for continuous strain sensing applications, Meas. Sci. Technol. **31**, 035109 (2020).

[41] P. Alonso Ruiz, Power dissipation in fractal Feynman–Sierpinski AC circuits, J. Math. Phys. **58**, 073503 (2017).

[42] J. P. Chen, L. G. Rogers, L. Anderson, U. Andrews, A. Brzoska, A. Coffey, H. Davis, L. Fisher, M. Hansalik, S. Loew, and A. Teplyae, Power dissipation in fractal AC circuits, J. Phys. A: Math. Theor. **50**, 325205 (2017).

[43] A. Muranova, On the notion of effective impedance, Oper. Matrices **2020**, 723 (2007).

[44] A. Muranova and R. Schippa, Eigenvalues of the normalized complex Laplacian on finite electrical networks, arXiv:2012.12759.

[45] A. Muranova, Effective impedance over ordered fields, J. Math. Phys. **62**, 033502 (2021).

[46] A. Muranova, On the effective impedance of finite and infinite networks, Potential Anal. **56**, 697 (2022).

[47] A. Muranova and W. Woess, Networks with complex weights: Green function and power series, Mathematics **10**, 820 (2022).

[48] R. S. Lakes, *Viscoelastic Materials* (Cambridge University Press, Cambridge, UK, 2009).

[49] B. Hoser and A. Geyer-Schulz, Eigenspectral analysis of Hermitian adjacency matrices for the analysis of group substructures, J. Math. Sociol. **29**, 265 (2005).

[50] Y. Tian and R. Lambiotte, Structural balance and random walks on complex networks with complex weights, arXiv:2307.01813 [SIAM J. Math. Data Sci. (to be published)].

[51] A. J. Noest, Phasor neural networks, in *Proceedings of the 1987 International Conference on Neural Information Processing Systems*, NIPS '87, edited by D. Anderson (Am. Inst. Phys., College Park, MD, USA, 1987), pp. 584–591.

[52] A. J. Noest, Discrete-state phasor neural networks, Phys. Rev. A **38**, 2196 (1988).

[53] A. J. Noest, Associative memory in sparse phasor neural networks, Europhys. Lett. **6**, 469 (1988).

[54] H. Leung and S. Haykin, The complex backpropagation algorithm, IEEE Trans. Signal Process. **39**, 2101 (1991).

[55] N. Benvenuto and F. Piazza, On the complex backpropagation algorithm, IEEE Trans. Signal Process. **40**, 967 (1992).

[56] M. Kobayashi, Exceptional reducibility of complex-valued neural networks, IEEE Trans. Neural Networks **21**, 1060 (2010).

[57] M. Kobayashi, Symmetric complex-valued Hopfield neural networks, IEEE Trans. Neural Netw. Learn. Syst. **28**, 1011 (2016).

[58] H. Zhang, M. Gu, X. D. Jiang, J. Thompson, H. Cai, S. Paesani, R. Santagati, A. Laing, Y. Zhang, M. H. Yung, Y. Z. Shi, F. K. Muhammad, G. Q. Lo, X. S. Luo, B. Dong, D. L. Kwong, L. C. Kwek, and A. Q. Liu, An optical neural chip for implementing complex-valued neural network, Nat. Commun. **12**, 457 (2021).

[59] J. Spall, X. Guo, and A. I. Lvovsky, Hybrid training of optical neural networks, Optica **9**, 803 (2022).

[60] X. Zhang, Y. He, N. Brugnone, M. Perlmutter, and M. J. Hirn, MagNet: A neural network for directed graphs, in *Advances in Neural Information Processing Systems 34: Annual Conference on Neural Information Processing Systems 2021, NeurIPS 2021, December 6–14, 2021*, edited by M. Ranzato, A. Beygelzimer, Y. N. Dauphin, P. Liang, and J. Wortman Vaughan (Curran Associates, Inc., 2021), Vol. 34, pp. 27003–27015.

[61] Y. He, M. Perlmutter, G. Reinert, and M. Cucuringu, MSGNN: A spectral graph neural network based on a novel magnetic signed Laplacian, in *Proceedings of the First Learning on Graphs Conference (LoG 2022)*, edited by B. Rieck and R. Pascanu, Proceedings of Machine Learning Research (MLR Press, 2022), Vol. 198, pp. 40:1–40:39.

[62] S. Furutani, T. Shibahara, M. Akiyama, K. Hato, and M. Aida, Graph signal processing for directed graphs based on the Hermitian Laplacian, in *Machine Learning and Knowledge Discovery in Databases — European Conference, ECML PKDD 2019, Würzburg, Germany, September 16–20, 2019, Proceedings, Part I*, edited by U. Brefeld, É. Fromont, A. Hotho, A. J. Knobbe, M. H. Maathuis, and C. Robardet (Springer-Verlag, Heidelberg, Germany, 2019), Vol. 11906, pp. 447–463.

[63] M. Cucuringu, H. Li, H. Sun, and L. Zanetti, Hermitian matrices for clustering directed graphs: Insights and applications, in *The 23rd International Conference on Artificial Intelligence and Statistics, AISTATS 2020, 26–28 August 2020, Online [Palermo, Sicily, Italy]*, Proceedings of Machine Learning Research, edited by S. Chiappa and R. Calandra (MLR Press, 2020), Vol. 108.

[64] R. Abdalla, Complex-valued neural networks—Theory and analysis, arXiv:2312.06087.

[65] M. Fanuel and R. Bardenet, Sparsification of the regularized magnetic Laplacian with multi-type spanning forests, arXiv:2208.14797.

[66] J. Liu and X. Li, Hermitian-adjacency matrices and Hermitian energies of mixed graphs, Lin. Alg. Appl. **466**, 182 (2015).

[67] K. Guo and B. Mohar, Hermitian adjacency matrix of digraphs and mixed graphs, J. Graph Theory **85**, 217 (2017).

[68] B. Mohar, A new kind of Hermitian matrices for digraphs, Lin. Alg. Appl. **584**, 343 (2020).

[69] S. Kubota, H. Sekido, and H. Yata, Periodicity of quantum walks defined by mixed paths and mixed cycles, Lin. Alg. Appl. **630**, 15 (2021).

[70] J. Biamonte, M. Faccin, and M. De Domenico, Complex networks from classical to quantum, Commun. Phys. **2**, 53 (2019).

[71] J. Nokkala, J. Piilo, and G. Bianconi, Complex quantum networks: A topical review, arXiv:2311.16265.

[72] M. Faccin, P. Migdał, T. H. Johnson, V. Bergholm, and J. D. Biamonte, Community detection in quantum complex networks, Phys. Rev. X **4**, 041012 (2014).

[73] B. Krawciw, L. D. Carr, and C. D. Behn, The small-world effect for interferometer networks, arXiv:2310.16451.

[74] G. Bianconi, The topological Dirac equation of networks and simplicial complexes, J. Phys.: Complex. **2**, 035022 (2021).

[75] G. Bianconi, Dirac gauge theory for topological spinors in 3+1 dimensional networks, J. Phys. A: Math. Theor. **56**, 275001 (2023).

[76] L. E. Hillberry, M. T. Jones, D. L. Vargas, P. Rall, N. Yunger Halpern, N. Bao, S. Notarnicola, S. Montangero, and L. D. Carr, Entangled quantum cellular automata, physical complexity, and Goldilocks rules, Quantum Sci. Technol. **6**, 045017 (2021).

[77] N. V. Vdovichenko, Spontaneous magnetization of a plane dipole lattice, Sov. Phys. JETP **21**, 350 (1965).

[78] T. Morita, Justification of Vdovichenko's method for the Ising model on a two-dimensional lattice, J. Phys. A: Math. Gen. **19**, 1197 (1986).

[79] T. Morita, Justification of Vdovichenko's method for the Ising model on a two-dimensional lattice, Prog. Theor. Phys. **83**, 701 (1990).

[80] S.-I. Amari, Learning patterns and pattern sequences by self-organizing nets of threshold elements, IEEE Trans. Comput. **C-21**, 1197 (1972).

[81] W. A. Little, The existence of persistent states in the brain, Math. Biosci. **19**, 101 (1974).

[82] J. J. Hopfield, Neural networks and physical systems with emergent collective computational abilities, Proc. Natl. Acad. Sci. USA **79**, 2554 (1982).

[83] J. E. Avron, A. Raveh, and B. Zur, Adiabatic quantum transport in multiply connected systems, Rev. Mod. Phys. **60**, 873 (1988).

[84] U. Smilansky, Discrete graphs—A paradigm model for quantum chaos, in *Chaos: Poincaré Seminar 2010*, edited by

B. Duplantier, S. Nonnenmacher, and V. Rivasseau (Springer-Verlag, Heidelberg, Germany, 2013), pp. 97–124.
[85] T. Peron, B. M. F. de Resende, F. A. Rodrigues, L. d. F. Costa, and J. A. Méndez-Bermúdez, Spacing ratio characterization of the spectra of directed random networks, Phys. Rev. E **102**, 062305 (2020).
[86] B. M. F. de Resende and L. d. F. Costa, Characterization and comparison of large directed networks through the spectra of the magnetic Laplacian, Chaos **30**, 073141 (2020).
[87] M. Fanuel, C. M. Alaíz, Ángela Fernández, and J. A. K. Suykens, Magnetic eigenmaps for the visualization of directed networks, Appl. Comput. Harmon. Anal. **44**, 189 (2018).
[88] Y. Lou and Y. Hong, Distributed surrounding design of target region with complex adjacency matrices, IEEE Trans. Autom. Control **60**, 283 (2014).
[89] J.-G. Dong and L. Lin, Laplacian matrices of general complex weighted directed graphs, Lin. Alg. Appl. **510**, 1 (2016).
[90] N. Masuda, M. A. Porter, and R. Lambiotte, Random walks and diffusion on networks, Phys. Rep. **716-717**, 1 (2017).
[91] M. A. Lohe, Non-Abelian Kuramoto models and synchronization, J. Phys. A: Math. Theor. **42**, 395101 (2009).
[92] M. A. Lohe, Quantum synchronization over quantum networks, J. Phys. A: Math. Theor. **43**, 465301 (2010).
[93] S.-H. Choi and S.-Y. Ha, Quantum synchronization of the Schrödinger–Lohe model, J. Phys. A: Math. Theor. **47**, 355104 (2014).
[94] S.-H. Choi, J. Cho, and S.-Y. Ha, Practical quantum synchronization for the Schrödinger–Lohe system, J. Phys. A: Math. Theor. **49**, 205203 (2016).
[95] P. Antonelli and D. N. Reynolds, Schrödinger–Lohe type models of quantum synchronization with nonidentical oscillators, J. Differ. Equ. **366**, 345 (2023).
[96] P. Van Mieghem, *Graph Spectra for Complex Networks*, 2nd ed. (Cambridge University Press, Cambridge, UK, 2023).
[97] J. M. Leinaas and J. Myrheim, On the theory of identical particles, Nuovo Cim. B **37**, 1 (1977).
[98] F. Wilczek, Magnetic flux, angular momentum, and statistics, Phys. Rev. Lett. **48**, 1144 (1982).
[99] F. Wilczek, Quantum mechanics of fractional-spin particles, Phys. Rev. Lett. **49**, 957 (1982).
[100] H. Bartolomei, M. Kumar, R. Bisognin, A. Marguerite, J.-M. Berroir, E. Bocquillon, B. Plaçais, A. Cavanna, Q. Dong, U. Gennser, Y. Jin, and G. Fève, Fractional statistics in anyon collisions, Science **368**, 173 (2020).
[101] J. Nakamura, S. Liang, G. C. Gardner, and M. J. Manfra, Direct observation of anyonic braiding statistics, Nat. Phys. **16**, 931 (2020).
[102] X. Li, Y. Shi, and I. Gutman, *Graph Energy* (Springer-Verlag, Heidelberg, Germany, 2012).
[103] O. Perron, Zur Theorie der Matrices, Math. Ann. **64**, 248 (1907).
[104] G. Frobenius, Über Matrizen aus nicht negativen Elementen, Sitzungsberichte der Königlich Preussischen Akademie der Wissenschaften **56**, 456 (1912).
[105] S. M. Rump, Perron–Frobenius theory for complex matrices, Lin. Alg. Appl. **363**, 251 (2003).
[106] D. Noutsos and R. S. Varga, On the Perron–Frobenius theory for complex matrices, Lin. Alg. Appl. **437**, 1071 (2012).
[107] L. Böttcher and H. J. Herrmann, *Computational Statistical Physics* (Cambridge University Press, Cambridge, UK, 2021).
[108] T. H. Cormen, C. E. Leiserson, R. L. Rivest, and C. Stein, *Introduction to Algorithms* (MIT Press, Cambridge, MA, USA, 2022).
[109] A. Solé-Ribalta, M. De Domenico, S. Gómez, and A. Arenas, Random walk centrality in interconnected multilayer networks, Physica D **323–324**, 73 (2016).
[110] See the repository https://gitlab.com/ComputationalScience/complex-weights.
[111] M. Faccin, T. Johnson, J. Biamonte, S. Kais, and P. Migdał, Degree distribution in quantum walks on complex networks, Phys. Rev. X **3**, 041007 (2013).
[112] R. Olfati-Saber, J. A. Fax, and R. M. Murray, Consensus and cooperation in networked multi-agent systems, Proc. IEEE **95**, 215 (2007).
[113] E. Estrada, *d*-path Laplacians and quantum transport on graphs, Mathematics **8**, 527 (2020).
[114] A. M. Childs, On the relationship between continuous-and discrete-time quantum walk, Commun. Math. Phys. **294**, 581 (2010).
[115] Y. Kuramoto, Self-entrainment of a population of coupled non-linear oscillators, in *International Symposium on Mathematical Problems in Theoretical Physics*, edited by H. Araki, Lecture Notes in Physics (Springer-Verlag, Heidelberg, Germany, 1975), Vol. 39, pp. 420–422.
[116] M. Lipton, R. Mirollo, and S. H. Strogatz, The Kuramoto model on a sphere: Explaining its low-dimensional dynamics with group theory and hyperbolic geometry, Chaos **31**, 093113 (2021).
[117] M. Thümler, S. G. M. Srinivas, M. Schröder, and M. Timme, Synchrony for weak coupling in the complexified Kuramoto model, Phys. Rev. Lett. **130**, 187201 (2023).
[118] H. Sakaguchi and Y. Kuramoto, A soluble active rotater model showing phase transitions via mutual entertainment, Prog. Theor. Phys. **76**, 576 (1986).
[119] R. Delabays, P. Jacquod, and F. Dörfler, The Kuramoto model on oriented and signed graphs, SIAM J. Appl. Dyn. Syst. **18**, 458 (2019).
[120] S.-Y. Ha and M.-J. Kang, On the basin of attractors for the unidirectionally coupled Kuramoto model in a ring, SIAM J. Appl. Math. **72**, 1549 (2012).
[121] F. A. Rodrigues, T. K. DM. Peron, P. Ji, and J. Kurths, The Kuramoto model in complex networks, Phys. Rep. **610**, 1 (2016).
[122] S.-Y. Ha, D. Ko, and Y. Zhang, Emergence of phase-locking in the Kuramoto model for identical oscillators with frustration, J. Appl. Dyn. Syst. **17**, 581 (2018).
[123] L. Q. English, Z. Zeng, and D. Mertens, Experimental study of synchronization of coupled electrical self-oscillators and comparison to the Sakaguchi–Kuramoto model, Phys. Rev. E **92**, 052912 (2015).
[124] E. Cozzo, M. Kivelä, M. De Domenico, A. Solé-Ribalta, A. Arenas, S. Gómez, M. A. Porter, and Y. Moreno, Structure of triadic relations in multiplex networks, New J. Phys. **17**, 073029 (2015).
[125] G. Costantini and M. Perugini, Generalization of clustering coefficients to signed correlation networks, PLoS One **9**, e88669 (2014).
[126] N. Masuda, M. Sakaki, T. Ezaki, and T. Watanabe, Clustering coefficients for correlation networks, Front. Neuroinform. **12**, 7 (2018).

[127] D. Cartwright and F. Harary, Structural balance: A generalization of Heider's theory, Psychol. Rev. **63**, 277 (1956).
[128] S. A. Marvel, J. Kleinberg, R. D. Kleinberg, and S. H. Strogatz, Continuous-time model of structural balance, Proc. Natl. Acad. Sci. USA **108**, 1771 (2011).
[129] E. Estrada, *The Structure of Complex Networks: Theory and Applications* (Oxford University Press, Oxford, UK, 2012).
[130] T. Maciążek and A. Sawicki, Non-Abelian quantum statistics on graphs, Commun. Math. Phys. **371**, 921 (2019).
[131] P. Erdős and A. Rényi, On Random Graphs I, Math. Debrecen **6**, 290 (1959).
[132] D. J. Watts and S. H. Strogatz, Collective dynamics of 'small-world' networks, Nature **393**, 440 (1998).
[133] A.-L. Barabási and R. Albert, Emergence of scaling in random networks, Science **286**, 509 (1999).
[134] J. W. Baron, Eigenvalue spectra and stability of directed complex networks, Phys. Rev. E **106**, 064302 (2022).
[135] T. Michoel and B. Nachtergaele, Alignment and integration of complex networks by hypergraph-based spectral clustering, Phys. Rev. E **86**, 056111 (2012).
[136] A. C. Schwarze and M. A. Porter, Motifs for processes on networks, SIAM J. Appl. Dyn. Syst. **20**, 2516 (2021).
[137] E. P. Wigner, On the distribution of the roots of certain symmetric matrices, Ann. Math. **67**, 325 (1958).
[138] Z. D. Bai and J. Yao, On the convergence of the spectral empirical process of Wigner matrices, Bernoulli **11**, 1059 (2005).